Tight-binding coherent-potential-approximation study of the electronic states of palladium—noble-metal alloys

P. M. Laufer and D. A. Papaconstantopoulos
Naval Research Laboratory, Washington, D.C. 20375-5000
(Received 9 October 1986)

We have performed calculations of the electronic states of palladium—noble-metal disordered alloys using an improved version of the tight-binding coherent-potential-approximation (TB-CPA) formalism. Our results for Pd-Ag are in excellent agreement with both experiment and the Korringa-Kohn-Rostoker (KKR) CPA. For Pd-Au we also obtain good agreement with specific-heat measurements. For Pd-Cu, probably due to charge-transfer effects, we do not obtain satisfactory agreement with experiment at the Cu-rich end. Our calculations indicate that if (a) highly accurate Slater-Koster parameters are used and (b) all the orbitals are included in the CPA conditions (i.e., not using a one-level TB model), the TB-CPA gives results that are equivalent to those of the KRR-CPA except in cases where off-diagonal disorder might be important.

I. INTRODUCTION

In the past few years there have been significant advances in our understanding of the electronic structure of disordered-alloy systems. The study of electronic states of random substitutional alloys is now considered commonplace. The coherent-potential approximation (CPA) introduced by Soven[1] which treats the alloy as an effective medium subject to zero average scattering has been employed extensively to achieve results which compare well with experiment. A recent review article by Faulkner[2] gives an excellent account of the development of the modern theory of alloys and gives detailed descriptions of various approaches along with critical assessments and comparisons of the results obtained from different theories with each other and experiment.

In particular, great strides have been made by researchers employing the Korringa-Kohn-Rostoker (KKR) CPA (Ref. 3) to perform calculations. This approach has supplanted the calculationally simpler tight-binding (TB) version of the CPA (Ref. 4) which was used in the early applications[5] of the CPA to real systems. Although the TB-CPA calculations gave results which were qualitatively correct, it was argued that it was not adequate for treating random hybridization and overlaps due to ambiguities in the Slater-Koster (SK) parameters. The KKR-CPA calculations then revealed detailed structure which was consistent with available experiment. Furthermore, the development of the spectral function formalism enabled one to attribute specific features to definite points in the Brillouin zone (BZ) and so follow their development through a series of alloys. These successes were taken as clear evidence of the superiority of the KKR approach.

In this paper, we aim to show that the TB-CPA, when employed properly, (i.e., all orbitals are treated on an equal footing and highly accurate SK fits to the band structures of the constituents are used), can be made to yield results on a par with those generated using the KKR-CPA. Moreover, the analysis of spectral functions is available in the TB formalism as well.

The plan of the paper is as follows: In the next section we review the CPA method and, in particular, the TB formalism. In Sec. III we discuss the details of the particular calculation, i.e., the improvements and shortcomings. The following sections deal with a detailed discussion of our densities of states and comparison with KKR calculations where available, with emphasis on Pd-Ag (Sec. IV), spectral functions (Sec. V) and specific heats (Sec. VI), and finally (Sec. VII) we discuss the implications and summarize our conclusions.

II. THE TIGHT-BINDING CPA FORMALISM

In this section we present the CPA as it is utilized within the TB approach. The CPA is a mean-field theory which within the single-site approximation requires that the scattering from impurities at the central site in the effective medium is zero on the average. The feature that distinguishes the CPA from the related average t-matrix approximation is that the effective medium is determined self-consistently in the CPA.

In the TB approach the Hamiltonian in question is written in terms of a matrix H_{ij}, where the elements are the interactions between states i and j in the expansion $\Psi=\sum_j C_j\phi_j(r)$ for one atom per unit cell, where $\phi_j(r)$ are Bloch functions. Then $\langle\Psi\,|\,H-E\,|\,\Psi\rangle=0$ leads to the determinantal equation which contains terms of the form $\langle\phi_{\alpha'}(r)\,|\,H\,|\,\phi_\alpha(r-R_n)\rangle$ which are treated as adjustable parameters. In our calculations the basis consists of nine Bloch sums created out of orbitals of s, p, and d symmetry.

The condition for zero average scattering is given by

$$C_A t_A + C_B t_B = 0 , \tag{1}$$

where t_A (t_B) is the scattering matrix for element A (B) and C_A (C_B) is the concentration of element A (B) present in the alloy. The scattering matrices t_i have the following form:

$$t_i=(\varepsilon_i-\Sigma)[1-(\varepsilon_i-\Sigma)G]^{-1} , \tag{2}$$

where ε_i is the matrix of the onsite SK parameters of the corresponding periodic Hamiltonian, Σ is the diagonal CPA self-energy matrix, and G is the Green's function defined as the following integral over the irreducible wedge of the BZ (IBZ):

$$G(z,\Sigma)=\int_{\mathrm{IBZ}} \frac{dk}{z-H(\Sigma,k)} , \tag{3}$$

where z is the complex energy and $H(\Sigma,k)$ is the 9×9 periodic Hamiltonian where the onsite parameters ε_i have been replaced by the self-energies Σ_i and the offsite parameters are determined from the constituents by virtual-crystal average. The preceding equations are solved self-consistently using a Newton-Raphson procedure to determine Σ and $G(z,\Sigma)$. Once $G(z,\Sigma)$ is known, the angular momentum decomposed densities of states (DOS) $N_l(E)$ can be calculated from the standard formula

$$N_l(E)=-\frac{1}{\pi}\lim_{z\to E^+}\mathrm{Im}\,\mathrm{Tr}G_l(z,\Sigma) ,$$

which can be further decomposed into site DOS as follows:

$$N_l^A(E)=-\frac{1}{\pi}\lim_{z\to E^+}\mathrm{Tr}\frac{[G_l^R+G_l^I(\Sigma-\varepsilon_B)]}{\varepsilon_B-\varepsilon_A} ,$$

where G_l^R and G_l^I are the real and imaginary parts of G, respectively.

In addition, the spectral density function $A(k,E)$ can also be obtained. This is analogous to the $E(k)$ function of the band structure in an ordered solid and is given by

$$A(k,E)=-\frac{1}{\pi}\mathrm{Im}\sum_l G_{ll}(k,E) .$$

The procedure described above differs from earlier TB-CPA calculations in three particulars. First, our SK Hamiltonians which are fit to self-consistent augmented-plane-wave (APW) calculations of the elements are much more accurate than those used by other workers. A typical rms error in the three-center orthogonal fits used here is 0.003 Ry. Second, unlike previous calculations which were done within the one-level TB model, our calculation uses four coupled CPA conditions corresponding to the s, p, t_{2g}, and e_g symmetries. Finally, the calculation of spectral densities was not included in earlier TB work,

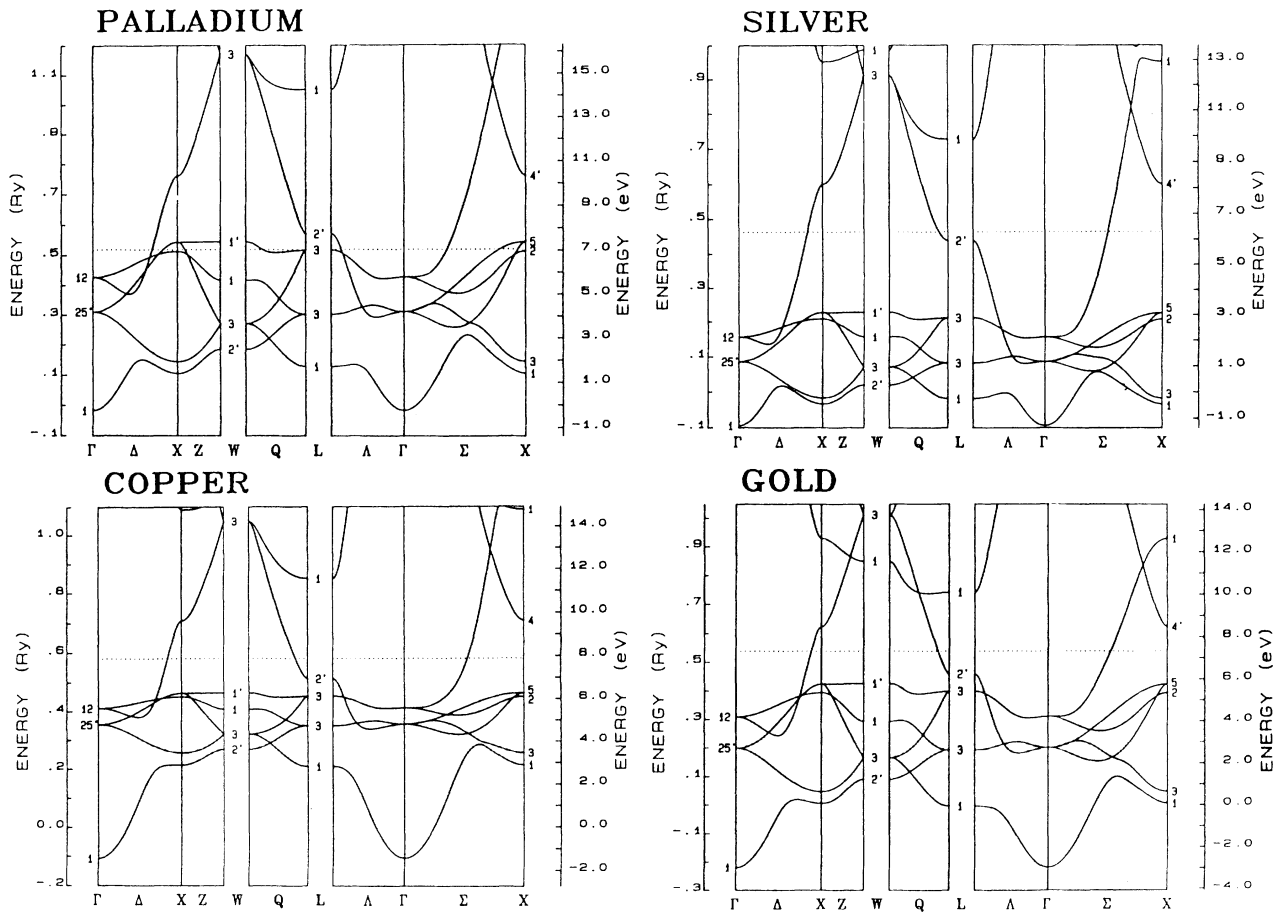

FIG. 1. Energy bands of the elements Pd, Cu, Ag, and Au.

thus helping create the misconception that they were unobtainable in the formalism.

The major shortcoming of this calculation is the neglect of off-diagonal disorder. The off-diagonal matrix elements are treated in a virtual crystal manner which is only adequate when the parameters of the constituents are similar.

An attempt to quantify this has been made by considering the root-mean-square difference between the 28 hopping integral parameters of the constituent elements. For Ag-Pd and Au-Pd this value is 10.0 and 9.5 mRy, respectively, while for Pd-Cu it is 34.5 mRy. This indicates that virtual-crystal averaging of the off-diagonal matrix elements may not be adequate to treat Cu-Pd, and that a more sophisticated treatment of the hopping will be necessary. In considering the band structures of the four constituent elements, (Fig. 1), a few features are worth noting. Ag differs from the others in that the d bands are significantly further from E_f than they are in the others. This leads to the more impressive split-band features of the Pd-Ag alloy. Copper differs from the others in the narrowness of the d bands as compared to the remaining three. This contributes to our expectations that the Cu-Pd calculation may not be as accurate as the others and that off-diagonal disorder need be incorporated.

III. DETAILS OF THE CALCULATIONS

The parameters for the TB Hamiltonians are derived as follows. We start with 32 three-center orthogonal parameters for the pure elements as given in Papaconstantopoulos.[6] These have been obtained through highly accurate SK fits (rms error less than 3 mRy for six bands) to first-principles band-structure calculations. For the elements used in this paper a self-consistent APW calculation, using the Hedin-Lundqvist form of the exchange potential, at 19 k points in the irreducible wedge of the BZ is used to get the bands in each iteration. For the SK fit a final APW run is used to generate eigenvalues at 33 k points in the IBZ. These SK fits are far superior to earlier sets of TB parameters. We then place the constituents on a common energy scale by shifting the onsite diagonal parameters such that the Fermi level (E_F) of each noble metal matches that of Palladium. (An alternate approach, i.e., matching the muffin-tin zeroes would yield an almost identical shift for these elements.) The CPA DOS are calculated on a mesh of 505 k points in the $\frac{1}{48}$ BZ. This particular k-point mesh gives DOS converged to within 3%.

The off-diagonal parameters, i.e., those representing transfer integrals, are obtained through a weighted average of the values of the pure elements at their equilibrium lattice spacing. These approximations amount to discounting off-diagonal disorder. We have found that a geometric average instead of an arithmetic one introduces small differences in our results in systems like Cu-Pd where the parameters of the constituents differ the most. We have also explored the effect of the variation of the lattice constant on the SK parameters by applying the scaling laws of Harrison and of Andersen *et al.*[7] The differences in the calculated DOS are negligible for Ag-Pd and Au-Pd, and somewhat (approximately 10%) larger for Cu-Pd. We have not done anything to account for the random distribution of nearest neighbors on the transfer integral other than averaging. As we have pointed out, we have indications, which will be borne out by our conclusions that this approximation is inadequate for the Pd-Cu system. We are working on implementing a scheme for including off-diagonal disorder within the TB approach.[8]

IV. DENSITIES OF STATES (DOS)

A. Palladium-Silver

The bands of palladium and silver (Fig. 1) differ in a feature that is of great importance in the following discussion. This is the position of the Γ_{12} and $\Gamma_{25'}$ states with respect to E_F in each material. The d states of palladium ($\Gamma_{12}^{\mathrm{Pd}}=-0.0926$ Ry and $\Gamma_{25'}^{\mathrm{Pd}}=-0.2098$ Ry) are situated at higher energies (closer to the E_F) than those of silver ($\Gamma_{12}^{\mathrm{Ag}}=-0.3070$ Ry and $\Gamma_{25'}^{\mathrm{Ag}}=-0.3773$ Ry). When the DOS of the elements Pd and Ag are compared, this feature shows up clearly, with the d bands of Ag lying below those of Pd with no significant overlap. Based on this observation we expect alloys of Pd with Ag to exhibit "splitband" behavior. This feature makes it clear that rigid band or virtual crystal approaches are inadequate. Further observation shows the distinct separation between t_{2g} and e_g features of the individual elements, strongly suggesting that the d bands cannot be treated jointly, but rather need be considered individually whilst not ignoring the coupling of these bands.

Figures 2 and 3 show the DOS (decomposed by site and angular momentum components) for two palladium-silver alloys. Note the development of the respective d band features as you compare $Pd_{0.80}Ag_{0.20}$ to $Pd_{0.20}Ag_{0.80}$. As expected the figures show clear split-band character with Pd d states lying above Ag and nearer the E_F. The following main features of the alloying should be noted: (1) the position of the main Ag and Pd peaks do not shift throughout the entire range. (2) With increasing Pd(Ag) concentration more structure is resolved in the Pd(Ag) d bands, and the width of the Pd(Ag) band broadens, and (3) increased alloying tends to make the spectrum less sharp as compared with the constituent spectra.

Recently Winter and Stocks[9] applied a method devised for doing fully self-consistent KKR-CPA calculations to the $Pd_{1-x}Ag_x$ system. In Figs. 4 and 5 we compare the DOS obtained in our calculations, with those obtained by them for $Pd_{0.80}Ag_{0.20}$ and $Pd_{0.50}Ag_{0.50}$. There are two panels in each figure, one for the Ag site DOS and the other for the Pd site. In Fig. 4 we see clearly the striking similarity in our results. The coinciding positions and relative heights of peaks and shoulders is truly remarkable. The only discrepancy is the low-energy fall off of the total Pd site DOS. Figure 5 is for 50% of each element—it is this concentration which is the severest test of our method. Focusing first on the Ag site we note that there are differences in the relative heights of individual peaks but not in their positions. As for structure, each total DOS has a peak at ~ 6 and ~ 4.5 eV below the E_F with a

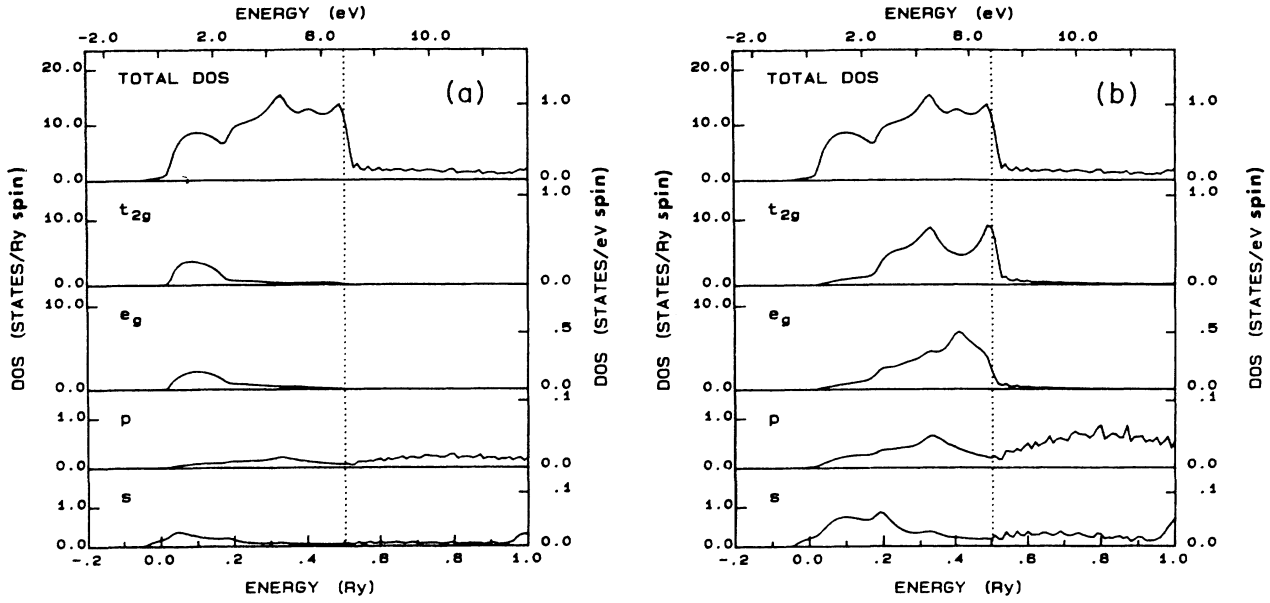

FIG. 2. Densities of states for $Pd_{0.80}Ag_{0.20}$. Ag site DOS shown in (a) and Pd site DOS shown in (b).

small shoulder followed by a tailing off out to E_F. Even the smallest qualitative detail is reproduced. For example, follow the e_g DOS (+) along in energy from −7 eV to E_F. At first it is zero and then increases and exhibits a small shoulder at −6.0 eV. This is followed by a relatively featureless flat region until −4.0 eV, where there is a small peak where it becomes marginally larger than the t_{2g} for a very brief range and then drops below again. From this point to E_F it roughly parallels the t_{2g} at slightly lower DOS. The t_{2g} has two peaks at −6.0 and −4.5 eV. The rest of t_{2g} can be understood from descriptions of e_g.

Now on the Pd site once again we see the clear similarities. The total Pd site DOS has two main features at about 1 and 3 eV below E_F, followed by a drop to a plateaulike region (as we go to lower energy) which then tails off to zero. The two calculations agree in all the qualitative features. The most spectacular manifestation of this is the crossing of the t_{2g} and e_g DOS at two points between 1 and 2 eV below the E_F.

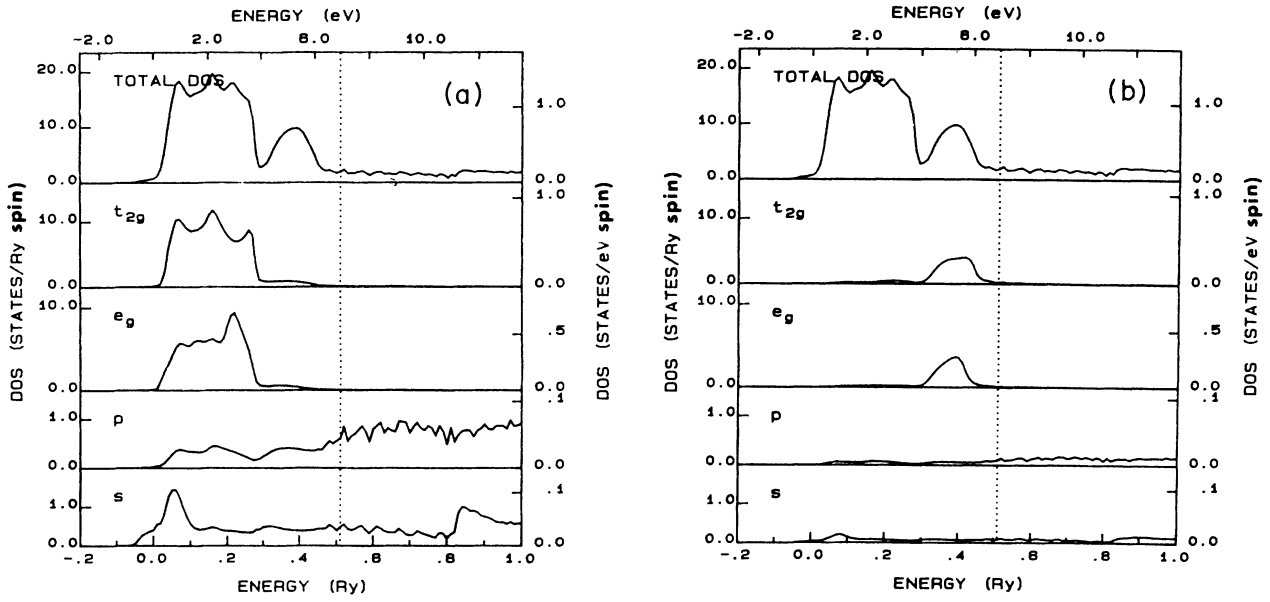

FIG. 3. Densities of states for $Pd_{0.20}Ag_{0.80}$. Ag site DOS shown in (a) and Pd site DOS shown in (b).

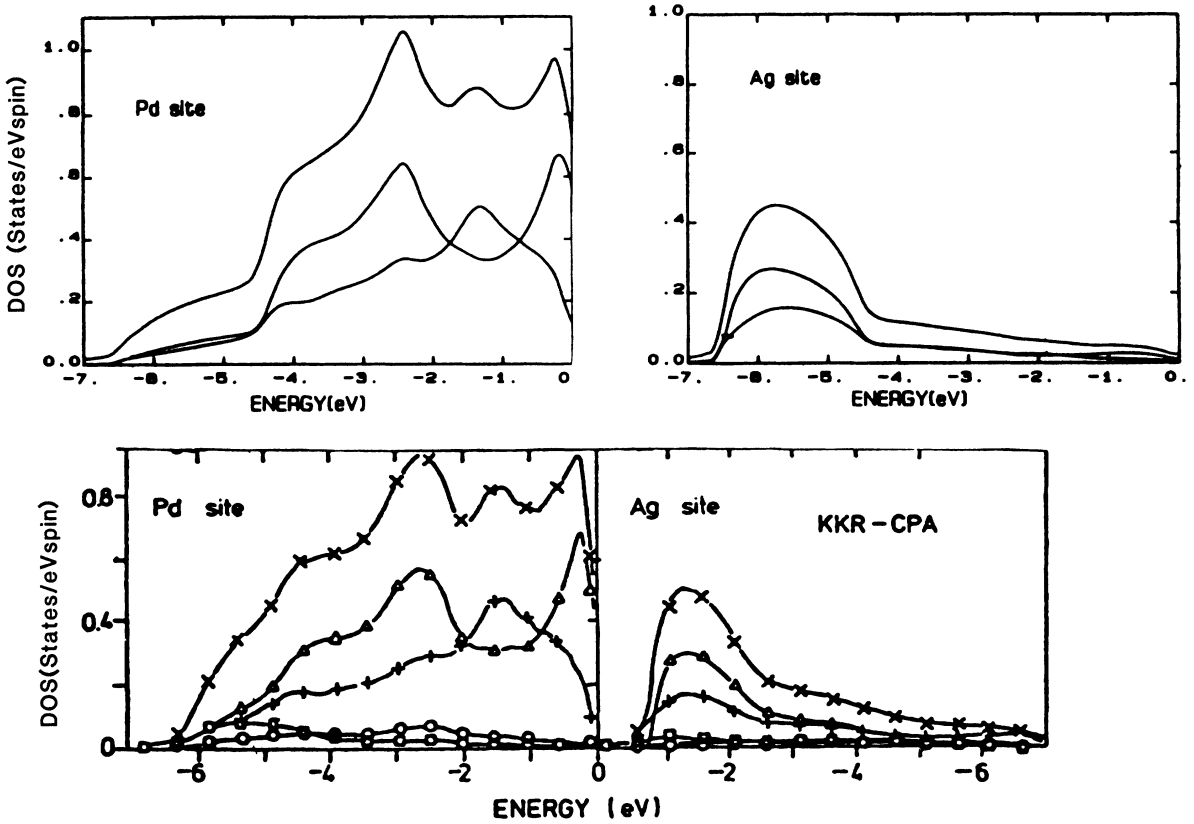

FIG. 4. Comparison of TB-CPA and KKR-CPA densities of states for $Pd_{0.8}Ag_{0.2}$. Total DOS, $\times$; t_{2g}, Δ; e_g, $+$.

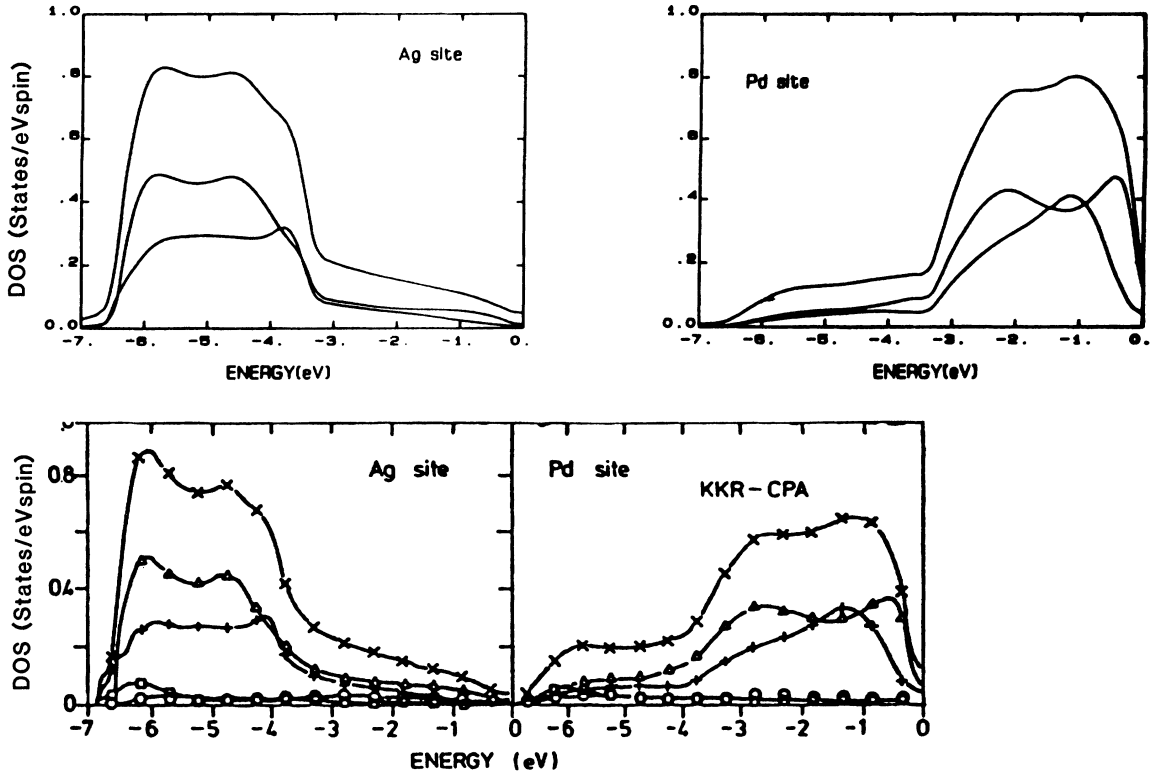

FIG. 5. Comparison of TB-CPA and KKR-CPA densities of states for $Pd_{0.5}Ag_{0.5}$. Total DOS, $\times$; t_{2g}, Δ; e_g, $+$.

B. Palladium-copper

Considering the band structures of pure Pd and Cu in Fig. 1 we find (with reference to E_F) $\Gamma_{12}^{Pd} = -0.0926$ Ry, $\Gamma_{25'}^{Pd} = -0.2098$ Ry, and $\Gamma_{12}^{Cu} = -0.1710$ Ry, $\Gamma_{25'}^{Cu} = -0.2250$ Ry. Unlike the Pd-Ag case we have overlap of the constituent d bands. However, a rigid band or virtual-crystal approach is still not adequate. Figures 6 and 7 depict the total and decomposed DOS for $Cu_{0.30}Pd_{0.70}$ and $Cu_{0.70}Pd_{0.30}$. It is evident from the figures that a common d band would not adequately describe this alloy.

The total DOS for the Pd rich composition shows many peaks, while that for the Cu rich ends shows only two. An important feature in this alloy is the precipitous decline in the total DOS in the neighborhood of the Fermi level. This makes $N(E_F)$ extremely sensitive to an accurate determination of E_F. Shifts as small as 10 mRy can change the value of $N(E_F)$ obtained by as much as a factor of 3. This point will be important when we discuss specific heat data in a later section. For the Pd-Cu alloy our calculations are restricted to $x < 0.30$ or $x > 0.70$, because the alloy forms in a different phase for the central concentration region.

The decomposed DOS show a Cu band which is broad and is essentially contained entirely in the range of the Pd-d bands even for low Cu concentrations. However, with increasing Cu in the alloy structure begins to manifest itself in the Cu spectrum. This structure is distinct from the Pd in that the peak positions and shapes clearly differ from those attributable to the Pd-rich end.

The Cu site d states show a double-peaked structure (see Fig. 7 $Cu_{0.70}Pd_{0.30}$), which drops to a small value as it approaches E_F. The low-lying peak exhibits a very sharp onset rising rapidly to the maximum value. The maximum of the higher-lying peak is clearly at a lower energy than the Pd peak in the immediate neighborhood of E_F. The Pd site DOS consists of a sharp peak near E_F which decreases quickly to a broad plateau as you go to lower energy, and finally tails off to zero at ~ 0.4 Ry below E_F.

Above E_F where the DOS are primarily s- and p-like there appears to be a great deal of noise in the calculation. We believe this is a numerical artifact due to the lack of d states in that region.

A comparison of total DOS for Cu-Pd alloys with a self-consistent KKR calculation of Winter *et al.*[10] yields the following. Although there is agreement in the general features, our results do not display the resemblance seen in Pd-Ag. The position of the Fermi energy does not agree, nor do we reproduce some of the finer details of the KKR calculation (such as relative peak heights). In addition, the KKR work finds the Cu d bands closer to E_F than the Pd d bands. This appears to be in contrast to our calculation and may be due to the effects of charge self-consistency and off-diagonal disorder that are not treated in our work. The position of the d resonance E_r is discussed in detail in Ref. 10; they find that for all their potentials $E_r^{Cu} > E_r^{Pd}$. However, the self-consistent potentials for pure Cu and Pd, that we are using, show that the d resonance of Cu is at -0.2255 Ry with respect to E_F while that of Pd is -0.1940 Ry, which means $E_r^{Cu} < E_r^{Pd}$ for the two ends of the compositional spectrum. In addition, one should note from Fig. 1 that away from Γ the Pd d states have strong contributions at E_F while those of Cu lie far away from E_F.

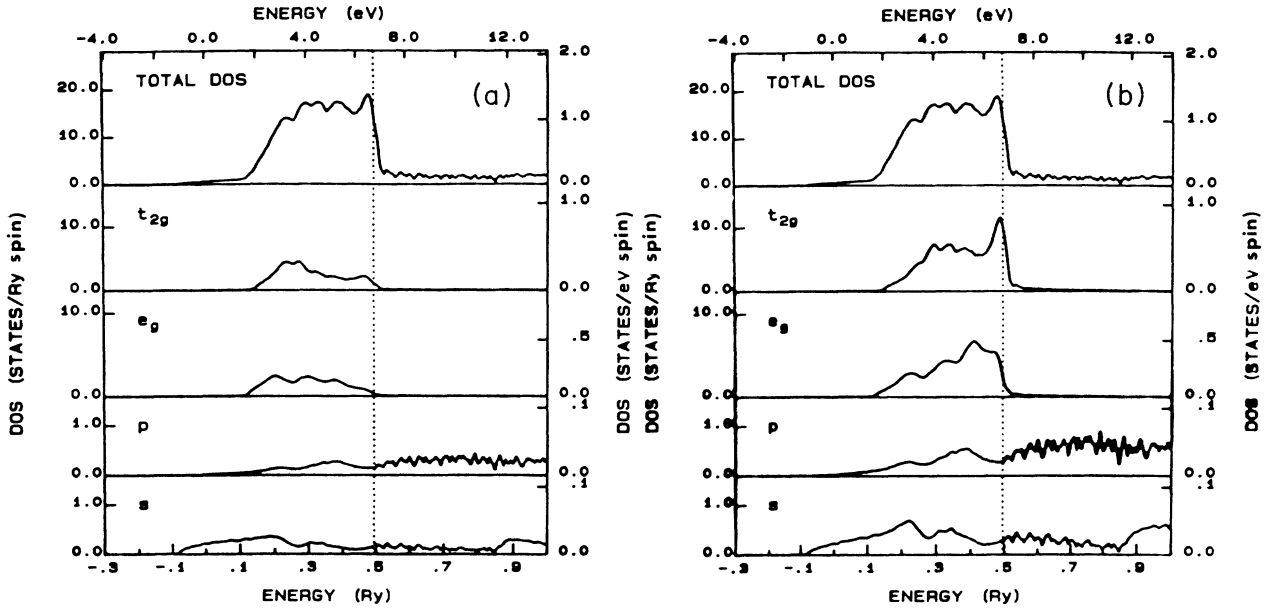

FIG. 6. Densities of states for $Cu_{0.3}Pd_{0.7}$. Cu site DOS shown in (a) and Pd site DOS shown in (b).

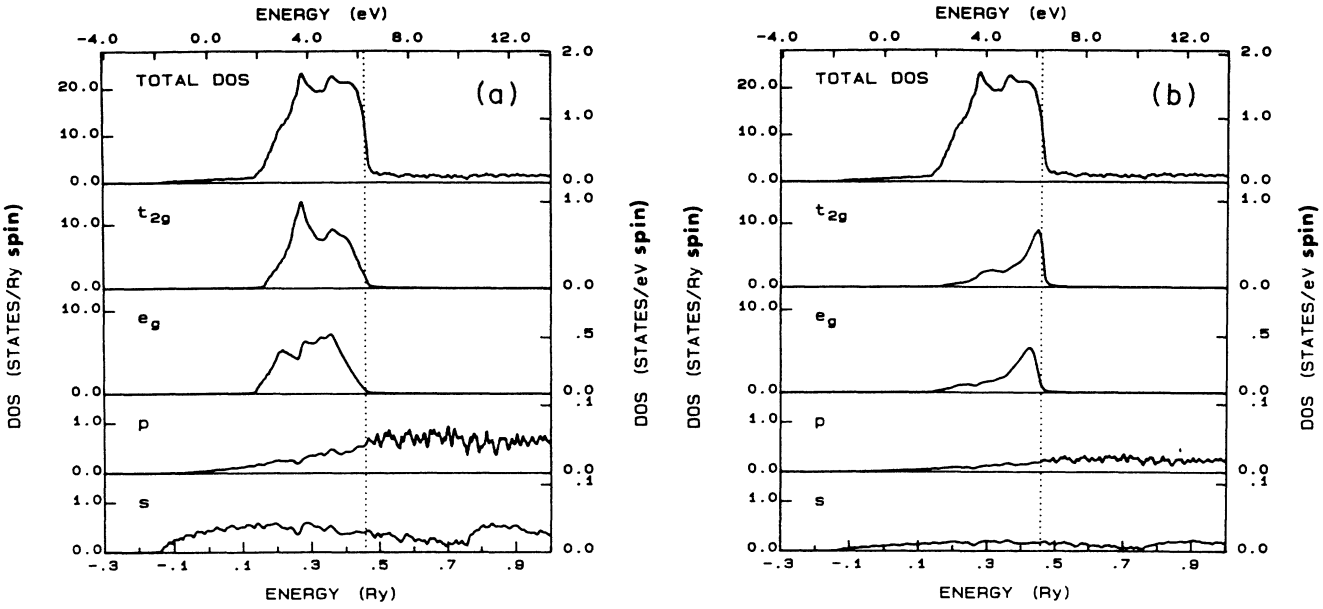

FIG. 7. Densities of states for $Cu_{0.7}Pd_{0.3}$. Cu site DOS shown in (a) and Pd site DOS shown in (b).

C. Palladium-gold

The values of Γ_{12}^{Au} and $\Gamma_{25'}^{Au}$ are -0.2284 Ry and -0.3391 Ry with respect to E_F. This would lead one to expect this alloy to be split-band like but not to the extent that we find for Pd-Ag. Although the total DOS of $Pd_{0.70}Au_{0.30}$ (Fig. 8) and $Pd_{0.30}Au_{0.70}$ (Fig. 9) do not differ in a qualitative manner, except for the position of E_F the decomposed DOS show that individual features are clearly attributable to either Pd or Au. This can be explained with reference to the band structures of Pd and Au (Fig. 1) where the similarity in band widths and relative positions can be noted, the major difference being the positions of E_F. In fact the DOS of pure Pd and pure Au

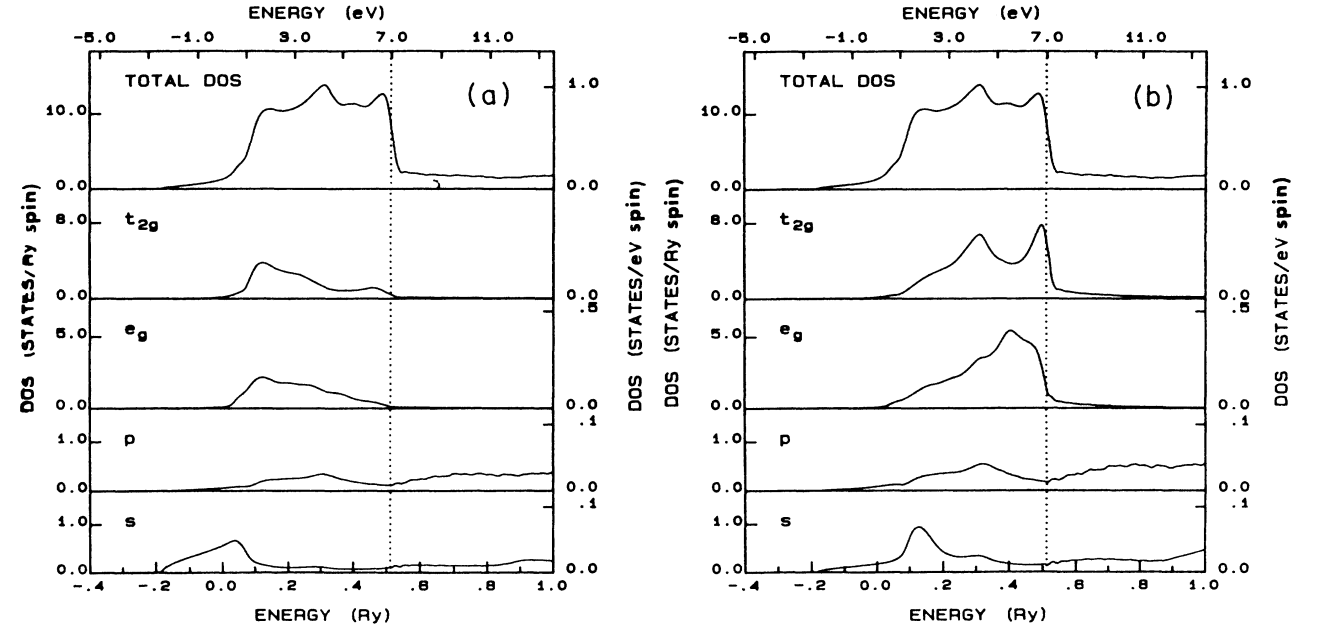

FIG. 8. Densities of states for $Pd_{0.7}Au_{0.3}$. Au site DOS shown in (a) and Pd site DOS shown in (b).

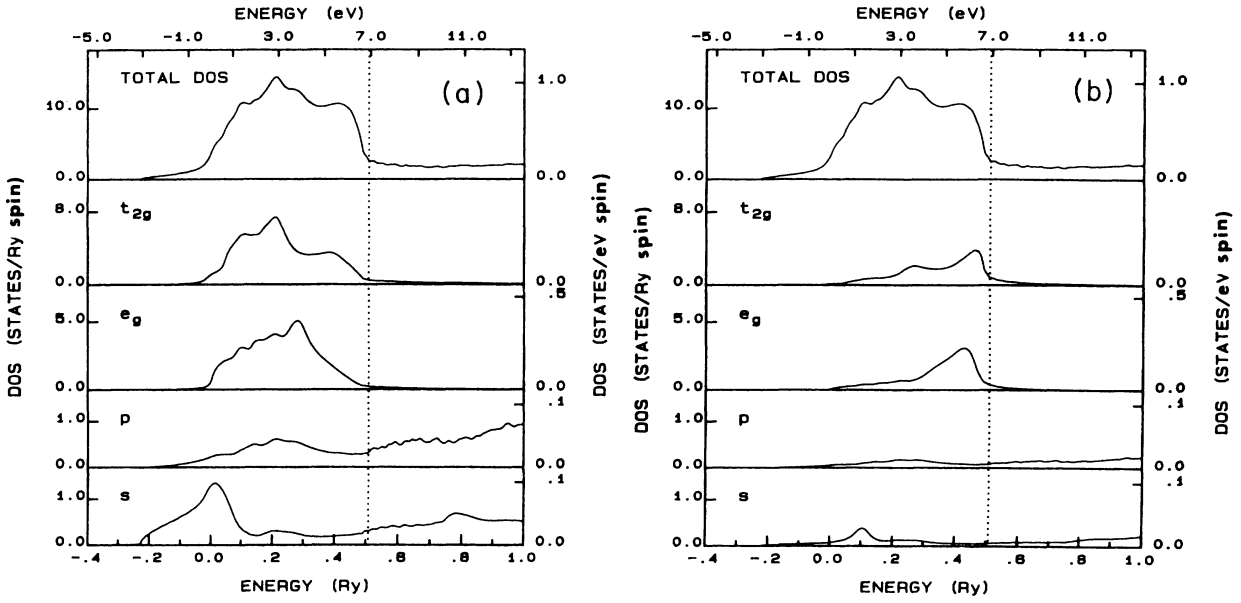

FIG. 9. Densities of states for $Pd_{0.3}Au_{0.7}$. Au site DOS shown in (a) and Pd site DOS shown in (b).

(Ref. 6) are very close if the position of E_F is disregarded.

In the alloy, the Pd-site d DOS consists of a sharp peak at ~ 0.5 Ry and another at ~ 0.3 Ry of t_{2g} character with a broad intervening valley. The e_g component has its major peak at about the center of this valley, and both then decrease as we go to lower energies.

The Au-site DOS for 70% Au shows a similar structure shifted down in energy at ~ 0.1 Ry. (The resemblance is far more dramatic at 90%.) The e_g component consists of an asymmetric peak skewed toward higher energies centered at ~ 0.3 Ry. The t_{2g} component consists of a peak at 0.4 Ry, another at 0.2 Ry followed by a shoulder, and finally declining to zero as we move away from E_F. Once again, as in the other Pd—noble-metal alloys, we find Pd states nearest the E_F. We remind the reader that in these alloys the neglect of the spin-orbit interaction in our calculation might introduce a significant error.

V. BLOCH SPECTRAL DENSITY

A. Palladium-silver

The Bloch spectral density $A(k,E)$ defined in Sec. II is plotted in Figs. 10 and 11 for Pd-Ag alloys, where each column has a fixed alloy concentration [from left to right Pd=0.2, 0.5, and 0.8]. In Fig. 10 the 5 rows are for five equally spaced k points along the Δ line, from Γ (0,0,0) to X(1,0,0). In Fig. 11 the five rows are for the three high symmetry points K,Γ,L and the two points equally spaced between the zone center (Γ) and the other two.

In an ordered solid $A(k,E)$ would be a set of infinitely sharp peaks where E is an allowed energy for a given k. Analogously for disordered systems $A(k,E)$ can be interpreted as an "alloy band structure."

The Γ point test demonstrates how we confirm the effects of alloying by tracing a specific feature of the component band structure. In the left-hand panel ($Pd_{0.2}Ag_{0.8}$) at Γ with reference to the bands of Ag and Pd we easily identify the second and third peaks to be $\Gamma_{25'}^{Ag}$ and Γ_{12}^{Ag}, respectively. This is followed by a featureless contribution at energies corresponding to the position of the d states in Pd. In the center panel ($Pd_{0.5}Ag_{0.5}$) the peaks at $\Gamma_{25'}^{Ag}$ and Γ_{12}^{Ag} have decreased in intensity, while the feature at higher energies has increased in intensity and is show-

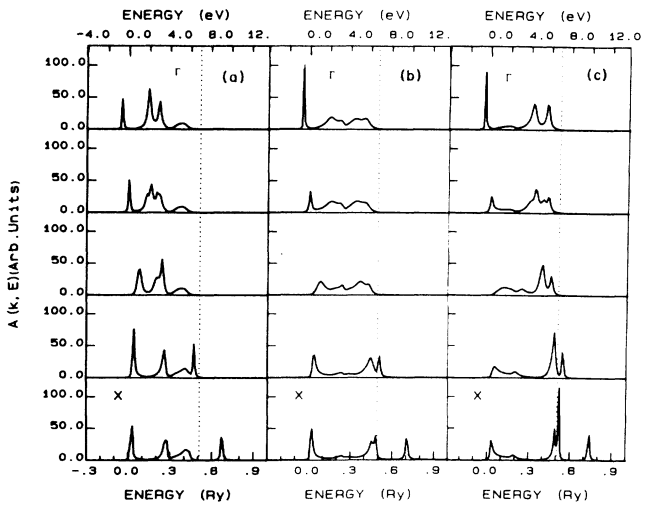

FIG. 10. Bloch spectral density along the Δ direction for Pd-Ag alloys. (a): $Pd_{0.2}Ag_{0.8}$. (b): $Pd_{0.5}Ag_{0.5}$. (c): $Pd_{0.8}Ag_{0.2}$.

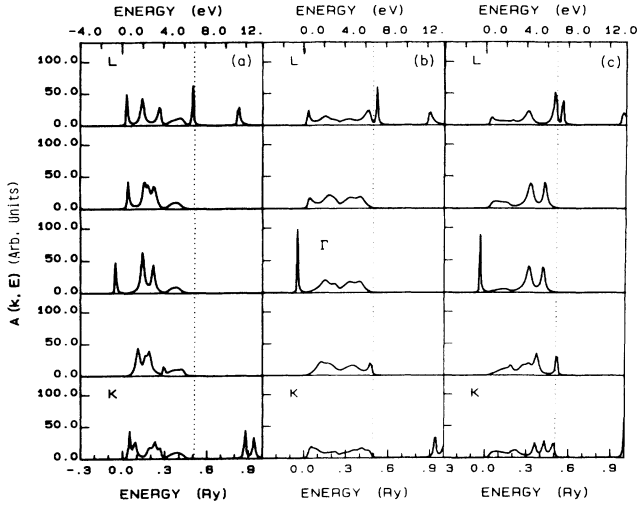

FIG. 11. Bloch spectral density at the symmetry points L, Γ, K, and two points in between for Pd-Ag alloys. Panels are as in Fig. 10.

ing what appears to be two distinct peaks. Owing to their position these are tentatively identified as Pd-d states $\Gamma_{25'}$ and Γ_{12}. This is confirmed when moving to the right-hand panel ($Pd_{0.8}Ag_{0.2}$), where we observe at the appropriate energies ($\Gamma_{25'}^{Pd}$ and Γ_{12}^{Pd}) more intense, well-defined peaks. In this instance the silver contribution has broadened and become featureless. Similar analysis can be made for other k points as well, but the high symmetry at Γ and the clear separation of the d levels make this the easiest to follow.

One can also follow a given "state" as it evolves along a high-symmetry line, e.g., from Γ to X by reading down a column. Another useful application of the spectral function is to fix E and let k vary; then, if $E=E_F$, $A(k,E_F)$ would be a representation of the Fermi surface. This amounts to reading down a "column" at fixed energy E_F using many "rows."

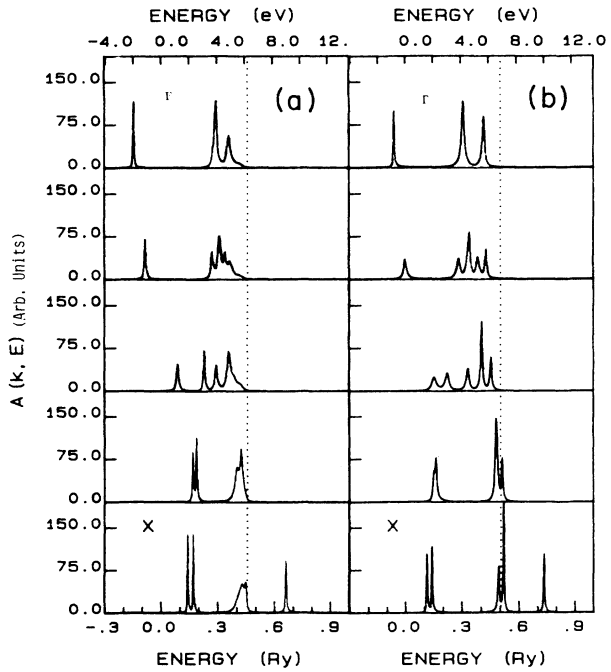

FIG. 12. Bloch spectral density along the Δ direction for Pd-Cu alloys. (a): $Pd_{0.20}Cu_{0.80}$. (b): $Pd_{0.8}Cu_{0.2}$.

B. Palladium-copper

Figure 12 shows Bloch spectral functions for $Pd_{0.20}Cu_{0.80}$ and $Pd_{0.80}Cu_{0.20}$ with the same configuration as Fig. 10. In this case the similarities in the spectral functions are more evident than the differences. Overall, the $Pd_{0.80}Cu_{0.20}$ and $Pd_{0.20}Cu_{0.80}$ are quite similar. This is another indication of the strong coupling of the Pd and Cu states and an indication that this interaction may have to be treated very carefully, including the effects of off-diagonal disorder.

VI. COMPARISON WITH EXPERIMENT

A. Electronic specific heats

The electronic specific heat coefficient γ is given by $\gamma=\frac{1}{3}\pi^2 k_B^2 N(E_F)$, where k_B is Boltzmann's constant and $N(E_F)$ is the electronic DOS evaluated at the E_F. This γ must be enhanced by a factor $(1+\lambda)$, where λ is known as the electron mass enhancement factor. For pure Pd[11], $\lambda\sim 0.4$ and for the noble metals $\lambda\sim 0.1$. In evaluating the enhancement factor $\lambda(x)$ for a given alloy we have used the following expression:

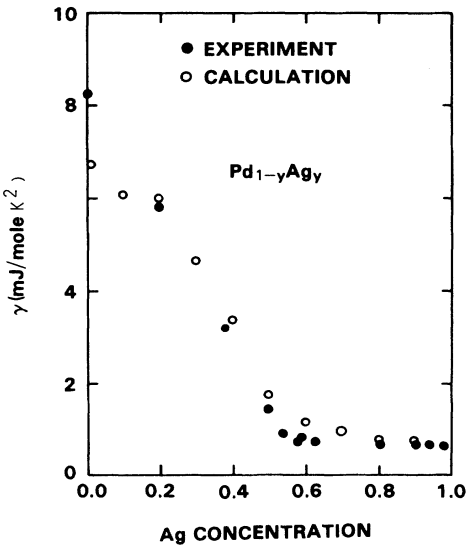

FIG. 13. Comparison of the calculated electronic specific heat coefficient γ, for Pd-Ag, to the measurements of Ref. 12.

TABLE I. Densities of states at E_F expressed in states (Ry spin).

	Pd				Noble metal				
	s	p	t_{2g}	e_g	s	p	t_{2g}	e_g	Total
$Pd_{0.1}Cu_{0.9}$	0.037	0.044	0.142	0.056	0.337	0.469	0.419	0.174	1.677
$Pd_{0.3}Cu_{0.7}$	0.144	0.170	6.638	0.959	0.354	0.486	1.612	0.375	10.740
$Pd_{0.7}Cu_{0.3}$	0.273	0.266	10.174	2.438	0.134	0.136	1.044	0.380	14.748
$Pd_{0.9}Cu_{0.1}$	0.280	0.245	9.637	2.759	0.033	0.031	0.335	0.094	13.415
$Pd_{0.1}Ag_{0.9}$	0.050	0.061	0.115	0.048	0.500	0.756	0.153	0.078	1.761
$Pd_{0.3}Ag_{0.7}$	0.145	0.133	0.549	0.234	0.427	0.455	0.168	0.085	2.196
$Pd_{0.5}Ag_{0.5}$	0.186	0.150	1.760	0.595	0.234	0.213	0.144	0.074	3.355
$Pd_{0.7}Ag_{0.3}$	0.224	0.203	6.413	1.299	0.113	0.116	0.185	0.058	8.611
$Pd_{0.9}Ag_{0.1}$	0.238	0.233	8.615	2.012	0.034	0.035	0.075	0.024	11.266
$Pd_{0.1}Au_{0.9}$	0.024	0.031	0.247	0.105	0.448	0.442	0.590	0.241	2.132
$Pd_{0.3}Au_{0.7}$	0.064	0.083	0.806	0.342	0.292	0.313	0.418	0.187	2.509
$Pd_{0.5}Au_{0.5}$	0.112	0.135	3.263	0.823	0.190	0.210	0.465	0.161	5.36
$Pd_{0.7}Au_{0.3}$	0.138	0.156	6.171	1.330	0.091	0.102	0.403	0.103	8.497
$Pd_{0.9}Au_{0.1}$	0.222	0.224	8.585	2.309	0.039	0.038	0.162	0.045	11.626

$$\lambda(x)=C_{\mathrm{Pd}}\frac{N_{\mathrm{Pd}}(x)}{N_{\mathrm{tot}}(x)}+C_{nm}\frac{N_{\mathrm{nm}}(x)}{N_{\mathrm{tot}}(x)}\ ,$$

where N_{tot} is the total DOS of the alloy at concentration x, N_{Pd} and N_{nm} are the Pd and noble-metal site DOS at E_F, and C_{Pd} and C_{nm} are constants fixed to give the correct λ at the pure Pd and noble-metal ends. In Table I we give the DOS values at E_F for several compositions of these alloys.

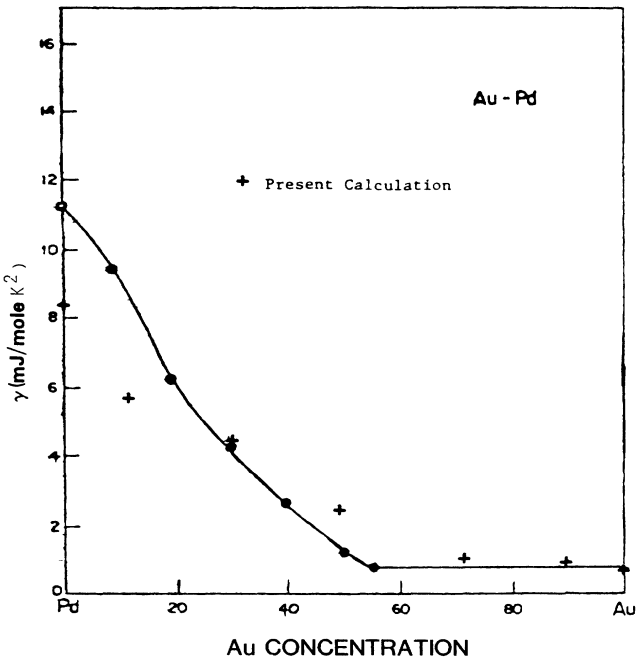

FIG. 14. Comparison of the calculated electronic specific heat coefficient γ, for Pd-Au, to the measurements of Ref. 14.

Figure 13 shows γ in mJ per mole K^2 versus at.% silver for the $Pd_{1-x}Ag_x$ system. The experimental results from Montgomery *et al.*[12] compare very nearly with our calculations. The main discrepancy occurs in the Pd-rich end of the spectrum and this is understandable as the contribution to λ^{Pd} due to paramagnons has not been included. For Cu-Pd our calculations at the Cu-rich end do not compare well with experiment.[13] However, because of the rapidly varying DOS in the neighborhood of E_F noted earlier, a very small shift of E_F would result in a much smaller $N(E_F)$. It is possible that the inclusion of off-diagonal disorder will yield a more accurate E_F and resolve this discrepancy.

Figure 14 presents γ for the Pd-Au system. The solid curve is derived from paramagnetic susceptibility data in Kim and Flanagan.[14] The crosses are our calculated values superimposed on their graph. In this system we see good agreement of our calculated γ with those derived from experiment.

B. Photoemission spectra

Norris and Myers[15] report photoemission experiments on a series of PdAg alloys. For the most part these experiments were carried out with incident photon energies $h\nu=10.2$ and 7.7 eV. The main findings are that the Pd peak at 2.1 eV below E_F and the Ag peak at 4.5 eV below E_F, each attributed to d states, does not shift position with alloying, and that the width of the Pd-d states increase with increasing Pd concentration at the Ag-rich end.

Our calculations are consistent with these findings as can be seen from our earlier descriptions. However, it should be noted that comparisons with electronic distribution curves based on photoelectron spectra, especially those of low energy, should not be carried too far as there is much distortion especially at low energies.[2]

VII. CONCLUSIONS

We have used a TB-CPA formalism to calculate the electronic states of Pd—noble-metal substitutional alloys. We have seen that this formalism when applied in an appropriate manner, yields results on a par with the more complex less economical (KKR) CPA. An extension of our TB-CPA to Pd—noble-metal hydrides[16] and also to other transition metal alloy hydrides[17] such as Ti-Nb-H, has yielded a picture of the electronic structure powerful enough to explain the superconducting behavior of these systems. In cases where there is little or no charge transfer or off-diagonal disorder effects the results are excellent. In instances where there are indications that the aforementioned need be considered, as in Pd-Cu, the overall features are still obtained but a more comprehensive theory needs to be implemented to get quantitative results. Work is in progress[8] on implementing a scheme which includes these effects within the TB formalism.

In light of these successes we maintain that the TB-CPA is a reliable and useful tool for investigating complex systems.

ACKNOWLEDGMENT

We wish to thank Dr. Warren E. Pickett for many useful discussions and suggestions.

[1]P. Soven, Phys. Rev. **156**, 809 (1967); **178**, 1136 (1969); J. L. Beeby, Proc. R. Soc. London, Ser. A **302**, 113 (1967).

[2]J. S. Faulkner, Prog. Mater. Sci. **27**, 1 (1982).

[3]G. M. Stocks, W. M. Temmerman, and B. L. Gyorffy, Phys. Rev. Lett. **41**, 339 (1978).

[4]J. S. Faulkner, Phys. Rev. B **13**, 2391 (1974).

[5]S. Kirkpatrick, B. Velicky, and H. Ehrenreich, Phys. Rev. B **4**, 3250 (1970); G. M. Stocks, R. W. Williams, and J. S. Faulkner, *ibid.* **4**, 4390 (1971).

[6]D. A. Papaconstantopoulos, *Handbook of the Band Structure of Elemental Solids* (Plenum, New York, 1986).

[7]W. A. Harrison, *Electronic Structure and the Properties of Solids*, (Freeman, San Francisco, 1980); O. K. Andersen, W. Klose, and H. Nohl, Phys. Rev. B **17**, 1209 (1978); J. D. Shore and D. A. Papaconstantopoulos, *ibid.* **35**, 1122 (1987).

[8]A. Gonis (private communication).

[9]H. Winter and G. M. Stocks, Phys. Rev. B **27**, 882 (1983).

[10]H. Winter, P. J. Durham, W. M. Temmerman, and G. M. Stocks, Phys. Rev. B **33**, 2370 (1986).

[11]D. A. Papaconstantopoulos, L. L. Boyer, B. M. Klein, A. R. Williams, V. L. Moruzzi, and J. F. Janak, Phys. Rev. B **15**, 4221 (1977); D. A. Papaconstantopoulos, B. M. Klein, E. N. Economou and, L L. Boyer *ibid.* **17**, 141 (1978).

[12]H. Montgomery, G. P. Pellis, and E. M. Wray, Proc. R. Soc. London, Ser. A **301**, 261 (1967).

[13]Y. Sato, J. M. Siversten, and L. E. Toth, Phys. Rev. B **1**, 1402 (1970).

[14]M. J. Kim and W. F. Flanagan, Acta Metall. **15**, 747 (1967).

[15]C. Norris and H. P. Myers, J. Phys. F **1**, 62 (1971).

[16]P. M. Laufer and D. A. Papaconstantopoulos, Phys. Rev. B **33**, 5134 (1986).

[17]D. A. Papaconstantopoulos and P. M. Laufer, J. Less-Common Met. **130**, 229 (1987).